AGU ADVANCING EARTH AND SPACE SCIENCE

Water Resources Research

RESEARCH ARTICLE
10.1029/2021WR030070

A Model for the Soil Freezing Characteristic Curve That Represents the Dominant Role of Salt Exclusion

S. K. Amankwah[1,2], A. M. Ireson[1,2], C. Maulé[2], R. Brannen[2], and S. A. Mathias[3]

[1]School of Environment and Sustainability, University of Saskatchewan, Saskatoon, SK, Canada, [2]Global Institute for Water Security, University of Saskatchewan, Saskatoon, SK, Canada, [3]Department of Engineering, Durham University, Durham, UK

Key Points:

- The soil freezing characteristic curve is an important property of frozen soils, and is required by cold regions hydrological models
- The Generalized Clapeyron Equation (GCE) is found to under predict freezing point depression
- A salt exclusion model and combined salt-GCE model perform well in simulating observed soil freezing characteristic curves

Correspondence to:

A. M. Ireson,
andrew.ireson@usask.ca

Citation:

Amankwah, S. K., Ireson, A. M., Maulé, C., Brannen, R., & Mathias, S. A. (2021). A model for the soil freezing characteristic curve that represents the dominant role of salt exclusion. *Water Resources Research*, *57*, e2021WR030070. https://doi.org/10.1029/2021WR030070

Received 26 MAR 2021
Accepted 28 JUL 2021

Abstract The phenomenon of freezing point depression in frozen soils results in the co-existence of ice and liquid water in soil pores at temperatures below 273.15 K (0°C), and is thought to have two causes: (a) capillary and adsorption effects, where the phase transition relationship is modified due to soil-air-water-ice interactions, and (b) solute effects, where the presence of salts lowers the freezing temperature. The soil freezing characteristic curve (SFC) characterizes the relationship between liquid water content and temperature in frozen soils. Most hydrological models represent the SFC using only capillary and adsorption effects with a relationship known as the Generalized Clapeyron Equation (GCE). In this study, we develop and test a salt exclusion model for characterizing the SFC, comparing this with the GCE-based model and a combined salt-GCE effect model. We test these models against measured SFCs in laboratory and field experiments with diverse soil textures and salinities. We consistently found that the GCE-based models under-predicted freezing-point depression. We were able to match the observations with the salt exclusion model and the combined model, suggesting that salinity is a dominant control on the SFC in real soils that always contain solutes. In modeling applications where the salinity is unknown, the soil bulk solute concentration can be treated as a single fitting parameter. Improved characterization of the SFC may result in improvements in coupled mass-heat transport models for simulating hydrological processes in cold regions, particularly the hydraulic properties of frozen soils and the hydraulic head in frozen soils that drives cryosuction.

Plain Language Summary When the ground freezes during the winter, not all the water stored in the soil turns into ice, which is because soil particles hold tightly onto some of the water making it impossible to freeze the water and because of the presence of dissolved salts within the soil pore water. The presence of unfrozen water in frozen soils determines the hydraulic properties of the soil which are vital for models of flood forecasting during spring melt, snowmelt infiltration for crop growth and the mechanical properties that determine the stability of the ground for infrastructure in cold regions. In this study, we use laboratory and field experiments, as well as different theoretical models to understand the effect of either or both dissolved salt and soil particles on the amount of unfrozen water stored in the frozen soil, and we suggest that dissolved salts may often be the dominant control. We propose a new relationship for this phenomenon that could improve cold regions hydrological models.

1. Introduction

The way that ice and liquid water are held in the soil pore space depends on the soil physical and chemical properties, the total water content and the temperature, and is expressed through a relationship known as the soil freezing characteristic curve (SFC). In cold regions, the SFC plays a significant role in heat, solute, and water transport (He et al., 2016; Spaans & Baker, 1996; Watanabe & Osada, 2017), which in turn influence winter evapotranspiration, snowmelt infiltration and runoff (Christensen et al., 2013; He et al., 2016), frost heave formation, thawing settlement, and frost depth penetration in frozen soils (Watanabe & Mizoguchi, 2002; Wen et al., 2012). Good knowledge of the properties of frozen soils is crucial in erosion control and flood risk assessment during spring melt in cold climates. In engineering, information about these properties are employed in infrastructure development such as the construction of roads, pavements, airport runways, bridges and railway lines. Further, in agronomy, these properties are useful in understanding microbial metabolism (He et al., 2016; Oquist et al., 2009; Watanabe & Osada, 2017) and crop water uptake in frozen soils as well as estimating water requirements for winter crops.

Spontaneous processes, such as the phase change process, occur to minimize free energy. Ice (i) and liquid water (l) can co-exist only when they have equal free energy, and this occurs at 273.15 K (0°C) (which is defined as T_0) for bulk water (Williams & Smith, 1989, p. 174, Zhang & Liu, 2018), where bulk water is defined as liquid water in an open container that is, solute free and at atmospheric pressure. Above T_0, liquid water has lower free energy than ice, and therefore liquid water is the stable phase. When the temperature of pure free water drops below T_0, the free energy of the liquid phase becomes higher than that of the solid phase driving the transformation of liquid water into ice, and ice becomes the stable phase. Unlike bulk water, soil pore water is found to freeze progressively with temperature as the temperature drops below T_0 (Hayashi, 2013; Williams & Smith, 1989, p. 175; Zhang & Liu, 2018), a phenomenon termed *freezing point depression*. This was first recognized by Schofield (1935) who used theoretical relationships between sub-zero temperature and matric potential as a means to extend observed soil moisture characteristic curves into drier soil conditions, where tensiometers fail. Early empirical observations of freezing point depression were provided by laboratory experiments reported by Koopmans and Miller (1966) and Williams (1970). Freezing point depression is understood to occur because, in any individual soil pore, the effects of solutes and the attractive forces generated with the soil solids (capillarity and adsorption forces, Jin et al., 2020) reduce the free energy of the liquid water, such that the temperature must be less than T_0 for the phase transition to occur. Freezing point depression is therefore attributed to (a) capillarity and adsorption effects (hereafter capillary effects, Spaans & Baker, 1996; Williams & Smith, 1989, p. 5; Zhou et al., 2018), and (b) the presence of salts (Williams & Smith, 1989, p 5; Williams, 1970, p. 16; Williams, 1964; Watanabe & Mizoguchi, 2002). The freezing temperature of the depressed liquid water in any individual pore is defined as T_f, (K). Both capillary effects and salt exclusion effects result in progressive freezing, which is to say the water in the continuum of soil pore spaces has a distribution of freezing temperatures and freezing occurs progressively as the temperature drops below T_0. However, the reason these effects are both progressive are different. In terms of capillary effects, the capillary and adsorptive forces and thus the freezing point of the water in an individual pore depends upon the pore size (analogous to matric potential), so smaller pores have lower freezing temperatures (Spaans, 1994). In terms of salts, during freezing, salts are excluded from the ice leaving the remaining solution more concentrated, and thus the freezing temperature of the remaining liquid water is further depressed (Banin & Anderson, 1974; Spaans & Baker, 1996; Williams, 1970, p. 17).

Freezing point depression is quantified at the soil continuum scale through the SFC. The SFC relates the volumetric liquid water content, θ_l (−), to temperature, $T\left(°C\right)$, in frozen soils and is analogous to the soil moisture characteristic curve (SMC), that relates liquid moisture content to matric potential, ψ (m) in unfrozen soils (Flerchinger et al., 2006; Koopmans & Miller, 1966; Spaans & Baker, 1996). The SFC can be directly measured for soils in the laboratory or the field by simultaneous measurements of liquid moisture content and soil temperature. Techniques to measure soil temperature and liquid water content have been reviewed elsewhere (Kelleners & Norton, 2012; Kelleners & Verma, 2010; Kelleners et al., 2009; Seyfried & Murdock, 2004; Susha Lekshmi et al., 2014). In frozen soils the bulk dielectric constant is insensitive to the presence of ice, which has a dielectric constant of around 3 (Kelleners & Norton, 2012), much lower than liquid water (~80), and hence dielectric soil moisture sensors can be used to measure the liquid water content in frozen soils. Kelleners and Norton (2012) measured the liquid water content of seasonally frozen soils in Wyoming using the Stevens HydraProbe (Stevens Water monitoring System Inc, 2007). The significant advantage of this instrument is that it simultaneously measures temperature and the liquid water content—thus directly measuring the SFC. The HydraProbe measures temperature using a thermistor embedded in the base plate of the sensor head (Kelleners & Norton, 2012; Seyfried & Murdock, 2004). Here, we will use the HydraProbes to measure SFCs in the laboratory.

Most models for the SFC that are used in coupled heat and mass transport models for frozen soils (e.g., Clark et al., 2015; Dall'Amico et al., 2011; Hansson et al., 2004; Painter & Karra, 2014) are based on predicting the SFC from the SMC using the Generalized Clapeyron Equation (GCE, Kurylyk & Watanabe, 2013; Williams & Smith, 1989). GCE based models assume that in frozen conditions the temperature predicts an equivalent effective soil matric potential, from which the liquid water content can be obtained from the SMC relationship (Mohammed et al., 2018; Teng, 2020; Zhang & Liu, 2018), and hence temperature is related to liquid water content. The advantage of this method is that there are no soil specific unknown parameters associated with the GCE relationship. However, this approach only represents capillary effects (Kurylyk & Watanabe, 2013) and does not account for the effects of solutes on the SFC (Azmatch et al., 2012). Given

that real soils do contain solutes this would seem to be a limitation with GCE based models, however, the relative significance of solute effects and capillary effects is not well documented or understood (Watanabe & Mizoguchi, 2002). There are extensive SFC datasets in the literature, from early work by Koopmans and Miller (1966) and Williams (1970) through to recent experimental work by Caicedo (2017), Schafer and Beier (2017), and Ren and Vanapalli (2019), (2020), and including papers where the solute effects are quantified (e.g., Patterson & Smith, 1985; Zhou et al., 2018). To validate the GCE model requires both observed SFC and SMC data, which are not present in all of these studies. Both Koopmans and Miller (1966) and Williams (1970) present data that shows that for some soils the GCE predicted SFC is consistent with the observed SFC and for others is not, and they suggest that where the GCE fails it may be due to solutes. Koopmans and Miller (1966) found that the GCE works better for finer soils, and suggested that for non-clay soils, a correction factor for the ratio of interfacial tension between water and soils versus water and ice can be applied to improve the predicted SFC. Gharedaghloo et al. (2020) adopted this approach to successfully map the SMC onto the SFC for a series of laboratory experiments, and they used pore scale simulations to demonstrate the differences in ice-entry during freezing versus air-entry during drying that this adjustment factor is designed to correct for. In contrast to this, Caicedo (2017) found that the GCE relationship fit SFC observations well for a fine sand and silt soil, while Ren and Vanapalli (2019) found that it did not fit observations well for two different clay soils. Spaans and Baker (1996) used a modified version of the GCE to account for osmotic potential (which the authors conclude is important at temperatures just below 273.15 K (0°C) and the temperature dependence of the latent heat of fusion. They suggest that their model matches observations, but they do not present SMC and SFC data independently, meaning that it is not clear how well the standard uncorrected GCE would perform. Schafer and Beier (2017) applied the Spaans and Baker (1996) model to a range of soils with mixed results, and suggest that limitations in performance maybe due to the presence of solutes. Zhou et al. (2018) extended the GCE to account for solute effects, and showed that their model was able to reproduce SFCs for saline soils from various laboratory experiments that were reported in the Chinese literature. In summary, the performance of the "standard" GCE model is mixed, and the instances where this model fails suggest it may not be a good model to adopt uncritically in coupled heat and mass transport models. Corrections that have been proposed for solutes or for differences in surface tension do not seem to work universally, and hence understandably have not been adopted in coupled models.

This study was designed to obtain both field and laboratory data that quantifies the SMC and SFC for different soil textures and salinities and to compare the results with those obtained from three different models: (a) capillary and adsorption effects (the GCE approach); (b) salt exclusion effects; (c) combined salt exclusion and GCE effects. In Section 2 we describe the laboratory and field experiments, and we present the three alternative models that were developed. In Section 3 we describe the results from the experiments and the performance of the alternative models to reproduce the observed data. Section 4 presents the conclusions where we provide a conceptual model for the behavior of seasonally frozen soils, and we provide recommendations for how to better represent the SFC in modeling studies.

2. Materials and Methods

2.1. Laboratory Experiments

The objective of the laboratory experiments was to measure the SMC and SFC of silica sand under controlled conditions. Silica sand was used with de-ionized water to give very low dissolved solutes in the pore water. The silica sand used was a fine-medium standard graded sand (ASTM C778 graded sand from Ottawa, Illinois Region, United States) with particle size ranging from 0.1 to 1 mm. The particle size was determined using the mechanical shaking method (Pekrioglu Balkis, 2019; Yan et al., 2017) with a set of sieves. The sand has a measured particle density of 2.5 g·cm^{-3}, an estimated bulk density of 1.45 g·cm^{-3}, and a porosity of 0.42. The particle density was measured using the pycnometer method as described by Pires et al. (2015), and the soil porosity was determined as the saturated volumetric moisture content of the soil. In both methods, adequate soil packing was achieved by carefully beating the sides of the soil container with a wooden meter rule until there was no change in the level of the sand in the container. If the level of the sand dropped, more sand was added, and the beating repeated. The bulk density of the sand was computed from the measured particle density and porosity.

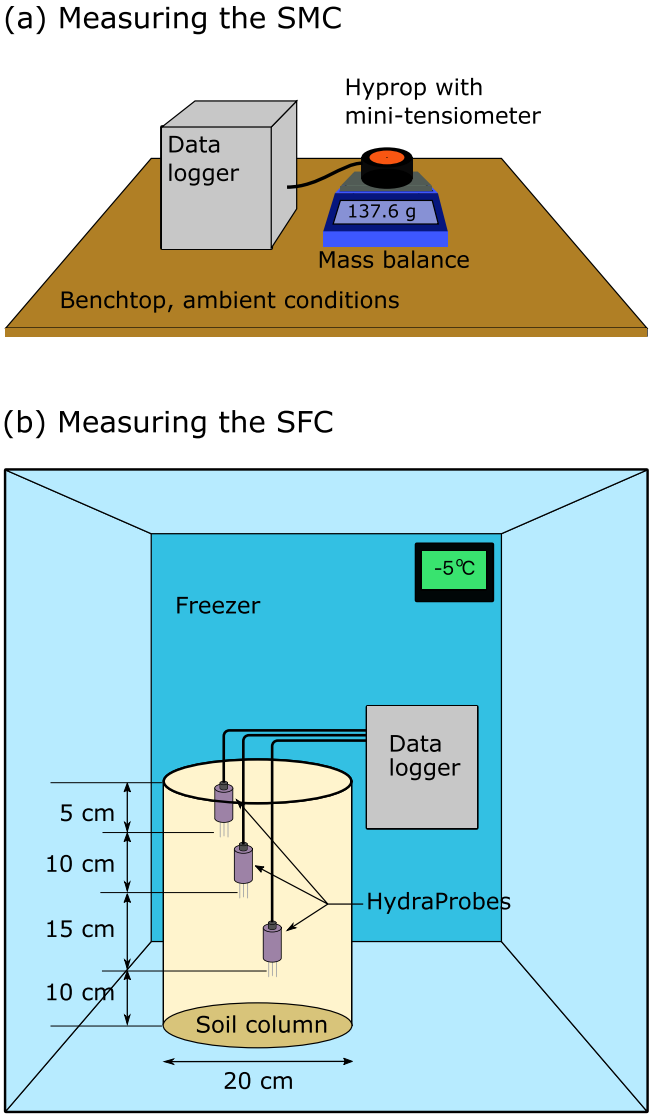

Figure 1. (a) Laboratory set-up for measuring the soil moisture characteristic curve, and (b) Laboratory set-up for measuring the soil freezing characteristic curve.

The SMC of the sand was measured using the HYPROP set-up (UMS GmBH in Munich, Germany) (Figure 1a). The sand was repacked into the sampling ring of the HYPROP using the same packing techniques as described in the previous paragraph. Following soil packing, the sample was saturated by placing the sampling ring in a bowl of de-aired distilled water for 24 h. After 24 h, the sampling ring was removed from the bowl and placed on top of the sensor unit of the equipment. The soil was then allowed to dry by evaporation. Soil moisture content and matric potential were measured simultaneously by the HYPROP using a mass balance (with an accuracy of ±0.001 g) and two vertically offset tensiometers (has an accuracy of ±0.015 m) (Breitmeyer & Fissel, 2017), respectively. Soil moisture and matric potential measurements were automatically logged at different time intervals.

The SFC of the same sand was measured using a soil column with dimensions 20 cm (diameter) by 40 cm (height) (Figure 1b). The column was made from PVC pipe with one end glued on to an acrylic plexiglass using a waterproof JB weld Epoxy. The column was insulated at the side with two layers of single-faced fiberglass to minimize horizontal temperature propagation through the column. The top of the column was left open so that freezing would begin from the surface of the soil. The bottom of the column was not insulated, but the acrylic plexiglass seal at the bottom of the column was thick enough to prevent freezing from beneath the columns. The soil was prepared at two different target moisture contents, 0.05 $m^3 \cdot m^{-3}$ and 0.24 $m^3 \cdot m^{-3}$ by thoroughly mixing by hand the appropriate amount of oven-dried soil and de-ionized water in a 34 liters (L) plastic container. For the saline treatments, the appropriate mass of salt was weighed and dissolved completely in the appropriate amount of de-ionized water before mixing with the soil. Sodium chloride salt (sodium chloride, crystalline from Fisher scientific) was used for this experiment. The total volume of soil (V_t), volume of water (V_w), target volumetric liquid moisture content (θ_l), mass of salt (m_s), bulk salt concentration ($c_b = m_S/V_t$) and pore water salt concentration ($c_s = m_s/V_w$) used for the freezing experiments are detailed in Table 1. The soil was then packed into the columns at 5 cm intervals and compacted with the base of a 250 ml flat bottom flask. Three pre-calibrated Stevens HydraProbes were inserted vertically into the soil at 5, 15, and 30 cm depths in the columns. The Stevens HydraProbe was used because of three reasons (a) it was readily available, (b) it can measure soil moisture content and temperature simultaneously, and (c) it is the same instrument used in our field experiments. The Stevens HydraProbe measures soil moisture content using the dielectric method, which relates the measured dielectric constant to the moisture content through a calibration equation (calibration equation

Table 1
Salt (NaCl) and Water Treatments Used in the Laboratory Freezing Experiment

Treatment	V_t(L)	θ_l($m^3 \cdot m^{-3}$)	V_w(L)	m_S(g)	c_b($g \cdot L^{-1}$)	c_s($g \cdot L^{-1}$)
1	12.58	0.05	0.629	0	0	0
2	12.58	0.05	0.629	1.258	0.1	2
3	12.58	0.05	0.629	5.032	0.4	8
4	12.58	0.05	0.629	10.064	0.8	16
5	12.58	0.24	3.0192	0	0	0
6	12.58	0.24	3.0192	6.038	0.48	2

specified by the Stevens Water monitoring System Inc, 2007). At each soil depth, a probe was inserted vertically into the soil, and the soil was packed around it. The probes were numbered according to their position within the column (probe 1 at 5 cm, probe 2 at 15 cm, and probe 3 at 30 cm, all from the start of the tines of the probes which are about 5.8 cm long). This was to ensure that the same probe was used at the same depth every time the SFC was measured. Following the soil packing, the columns were covered with a polyethylene sheet to prevent evaporation and allowed to sit for two days for moisture to equilibrate in the columns. The columns were then placed in a freezer to measure the SFC. For every treatment, both the freezing and thawing curves were measured. For the freezing runs, the temperature of the freezer was set constantly at 268.15 K. The soil was allowed to freeze until the temperature of all the soil depths approached the freezer temperature or when the moisture content stayed constant. Afterwards, the temperature of the freezer was raised to and kept constant at 277.15 K for the soil to thaw. The thawing runs were terminated when all the soil depths reached a temperature greater than 273.15 K. Soil moisture content ($m^3 \cdot m^{-3}$) and temperature data (K) were logged every minute using a CR 3000 series data logger from Campbell Scientific.

2.2. Field Experiments

The objective of the field study was to measure the SMC and SFC for different in situ soils with varying texture and salinity. The field studies were conducted at the St Denis National Wildlife Area (SDN) in the Canadian prairies (Bam & Ireson, 2019; Bam et al., 2019) and the Boreal Ecosystem Research and Monitoring Sites (BERMS) Old Jack Pine (OJP) site in the boreal plans ecozone in Saskatchewan (Ireson et al., 2015; Nazarbakhsh et al., 2020).

The SDN field site is located in the semi-arid, cold Canadian prairies ecozone about 40 km east (106° 5′ 36″ W, 52° 12′ 34″ N) of Saskatoon, Saskatchewan (Hayashi et al., 1998; Nachshon et al., 2014). The site is partly cropped with wheat, barley, and canola while the rest of the vegetation is a combination of native and introduced grasses (Bam et al., 2019; Hayashi et al., 1998). The site is characterized by an undulating hummocky topography (Bam et al., 2019; Hayashi et al., 1998; Nachshon et al., 2014) with silty stratified sediments and glacial tills (Bam et al., 2019; Hayashi et al., 1998; Nachshon et al., 2014). Soils at SDN can be high in salt, particularly sulphate salts (Nachshon et al., 2014). The site experiences mean annual precipitation (1967–1996) of 358 mm, of which 74 mm occurs as snow (November–April) (Budhathoki, 2018). The mean monthly air temperature for the site is 258.45 K (−14.7°C) for January and February and 291.85 K (18.7°C) for July and August (Bam & Ireson, 2019). At SDN, soil moisture data were measured on a transect with three soil profiles, namely upslope, mid-slope, and downslope. In this study, however, only observation from the upslope profile is used. Data sets used in the SDN analysis include time series data of soil moisture content ($m^3\ m^{-3}$), soil temperature (K), and matric potential (m) at 5 cm, 20 and 50 cm depths. The soil moisture content and soil temperature were measured using Stevens HydraProbes from Campbell Scientific inserted vertically in the soil at the different soil depths. These HydraProbes are the same as those used in the laboratory experiments. The soil matric potential was measured using the 229 heat dissipation matric water potential sensor from Campbell Scientific.

The OJP site is located east of Prince Albert National Park in the southern Canadian Boreal Forest (104.69°W, 53.92°N), Saskatchewan, Canada (Nazarbakhsh et al., 2020). As the name implies, the OJP site is dominated by jack pine (*Pinus banksiana Lamb.)* with an understory of reindeer lichen (*Cladonin* spp.) (Barr et al., 2012; Nazarbakhsh et al., 2020). The soil at OJP is a well-drained sandy soil (Barr et al., 2012; Nazarbakhsh et al., 2020) with a water table depth of at least 5 m below the soil surface (Barr et al., 2012). The OJP site receives an average precipitation of 307 mm (Nazarbakhsh et al., 2020). It is estimated that about 21% to 31% of the total precipitation at this site occurs as snow (Ireson et al., 2015; Nazarbakhsh et al., 2020). The site experiences a mean monthly air temperature of around 263.15 K (−10°C) in January and 293.15 K (20°C) in July (Nazarbakhsh et al., 2020). For the OJP site, soil moisture content and soil temperature were measured at different soil depths with a Campbell Scientific 615 soil moisture sensor and a Type-T (copper/constantan) thermocouples, respectively. In this study, soil temperature data at 5 cm depth and moisture content data at the top 15 cm were used. The reason is that the soils at the OJP site do not freeze much below 15 cm, which could be because the trees and understory provide insulation that keeps the soil warm. This site also does not have matric potential measurements, which are needed for establishing the SMC. As such, SMC data set published by Cuenca et al. (1997) for the same field site was used in this study. Cuenca

et al. (1997) measured moisture content using both the neutron probe (Campbell Pacific Nuclear 503 Hydroprobe) and the TDR. Soil matric potential was also measured using a combination of in situ tension disk infiltrometers and water retention data from the laboratory (measured using soil cores). These experiments are described in detail by Cuenca et al. (1997). The raw data points were extracted from the original plot using WebPlotDigitizer (Version 4.2) (Rohatgi, 2015).

2.3. Modeling

As noted earlier, two possible causes of freezing point depression in soils have been identified: (a) capillary effects (capillarity and adsorption effects on the free-energy of the pore-water, which is related to the soil pore-size distribution); and (b) solute effects (the effect of dissolved salts on the freezing temperature of free water, independent of the soil pore-size distribution). In this study, models are applied to simulate the soil freezing characteristic curve assuming: (a) capillary effects alone; (b) salt exclusion effects alone; and (c) combined capillary and solute effects.

Note that here, the unit of temperature is always in Kelvin. The freezing temperature for free pure water at atmospheric pressure is denoted T_0 and has a value of 273.15 K (0°C). The freezing temperature of water in a specific part of the soil pore space is denoted T_f. For convenience, we plot SFC curves using the freezing point depression of soil water, denoted T_d and defined as

$$T_d = T_f - T_0 \tag{1}$$

2.3.1. GCE Model

When two phases of a pure substance (e.g., water and ice) are in equilibrium with one another, the temperature and Gibbs free energy (expressed here on a per unit mass basis), G (J·kg^{-1}), of each phase must be the same, though the pressures, P (Pa), may differ (e.g., consider liquid water and water vapor at the water-air interface in a capillary tube). When there is a change in temperature or pressure a new equilibrium state will be reached, again with identical T and G in each phase, such that the change in Gibbs free energy, dG must also be the same for each phase. The change in Gibbs free energy is given by (Williams & Smith, 1989, p. 186 and 190)

$$dG = -sdT + \nu dP \tag{2}$$

where s (J·K^{-1}· kg^{-1}) is entropy and ν is specific volume (m^3·kg^{-1}). Hence for ice (subscript i) and liquid water (subscript l) we can write

$$\nu_l\, dP_l - \nu_i\, dP_i = \left(s_l - s_i\right) dT \tag{3}$$

During phase change, the change in entropy is due to the consumption or release of latent heat, so that (Williams & Smith, 1989, p. 190, p. 190)

$$s_l - s_i = \frac{L}{T} \tag{4}$$

where L (J kg^{-1}) is the latent heat of fusion. Hence we have

$$\nu_l\, dP_l - \nu_i\, dP_i = \frac{L}{T} dT \tag{5}$$

Equation 5 is not controversial in the literature, but different assumptions have been made about how to deal with the ice pressure, P_i (Kurylyk & Watanabe, 2013). Here we will adopt the most common assumption for this (Clark et al., 2015; Dall'Amico et al., 2011; Hansson et al., 2004; Hayashi, 2013; Painter & Karra, 2014; Williams & Smith, 1989) which is that there is no change in ice pressure, $dP_i = 0$. Noting that the density of water, ρ_l (kg·m^{-3}) is equal to 1 / ν_l, we have

$$\frac{dP_l}{dT} = \rho_l \frac{L}{T} \tag{6}$$

Table 2
Freezing Point Depression for an Aqueous NaCl Solution

Salt mass X (%)	1	5	10	15	18
$T_m\left(K\right)$	−0.58	−3.04	−6.79	−11.02	−14.29

Note. Here T_m (K) is the minimum temperature below T_0 where only liquid water is present, for a given mass concentration of NaCl.

Matric potential, ψ (m), is defined from the relationship $P_l = \psi\rho_l g$, where g $(m.s^{-2})$ is gravitational acceleration. Hence we have

$$\frac{d\psi}{dT} = \frac{L}{Tg} \tag{7}$$

Integrating this equation between $\left(T = T_0, \psi = 0\right)$ and $\left(T = T_f, \psi = \psi_f\right)$, we have

$$\psi_f = \frac{L}{g}\ln\left(\frac{T_f}{T_0}\right) = \frac{L}{g}\ln\left(\frac{T_0 + T_d}{T_0}\right) \tag{8}$$

Equation 8 is approximately equal to $\psi_f = L / g\left(T_d / T_0\right)$ (since $\ln\left(1 + x\right) \approx x$, Kurylyk & Watanabe, 2013) i.e., a linear relationship between matric potential and temperature, that predicts a matric potential of −124 m for a temperature of −1 K (Hayashi, 2013). Here we use non-linear form in Equation 8 since it will be important in our combined model below. If the soil is partially saturated at the time of freezing, the matric potential will be less than zero. Let ψ_u (m) represent the equivalent unfrozen matric potential, which is related to the total water content (ice plus liquid), and is not necessarily constant in frozen soil conditions (total water content changes due to movement of liquid water, which can also refreeze in the soil and hence result in an accumulation of ice that the dielectric probes will not register). Ice will only form in the pore space when $\psi_f < \psi_u$. Hence, we have

$$\psi_l = \begin{cases} \psi_u & \psi_f \geq \psi_u \\ \dfrac{L}{g}\ln\left(\dfrac{T_0 + T_d}{T_0}\right) & \psi_f < \psi_u \end{cases} \tag{9}$$

where ψ_l predicts the liquid water content, θ_l $(m^3 \cdot m^{-3})$, given here by the van Genuchten equation (VGN) (Kelleners & Norton, 2012; van Genuchten, 1980).

$$\theta_l = \theta_r + \left(\theta_s - \theta_r\right)\left(1 + \left(\alpha\psi_l\right)^n\right)^{-m} \tag{10}$$

where θ_r $(m^3 \cdot m^{-3})$ is the residual moisture content, and θ_s $(m^3 \cdot m^{-3})$ is the saturated moisture content or porosity, $\alpha\left(m^{-1}\right)$ is approximately the inverse of the air entry matric potential, n and m are dimensionless empirical shape-defining parameters. Note that the total water content of the soil, θ_t $(m^3 \cdot m^{-3})$, ignoring changes in density of ice versus water, is given by

$$\theta_t = \theta_r + \left(\theta_s - \theta_r\right)\left(1 + \left(\alpha\psi_u\right)^n\right)^{-m} \tag{11}$$

and the ice content, θ_i $(m^3\ m^{-3})$ is given by

$$\theta_i = \theta_t - \theta_l \tag{12}$$

such that when $\psi_f \geq \psi_u$ then $\theta_t = \theta_l$ and $\theta_i = 0$.

Combining Equations 9 and 10 results in an SFC relationship between temperature and liquid water content, and this method describes the GCE model discussed in the introduction.

2.3.2. Salt Exclusion Model

In free-water saline solutions, the freezing temperature is depressed below T_0 due to the presence of solutes. Let T_m (K) represent the temperature below T_0 at which a saline solution of a given concentration will freeze (i.e., T_m is for salt exclusion what T_d is for the GCE model). Moreover, during freezing, salts are excluded from the ice phase, making the remaining solution more concentrated, leading to a further depression in the freezing point of the remaining liquid water (Banin & Anderson, 1974).

Here, we develop a salt exclusion model for NaCl. The same procedure could be applied to different salts where freezing point depression data are available. Table 2 shows observed data from Haghighi et al. (2008) for salt concentration against freezing point depression for sodium chloride salt.

Table 3
Arbitrary Soil Parameters Used in the Model Simulations

VGN parameters	Value
$\alpha\,(\mathrm{m}^{-1})$	−4.79
n	5
m	0.8
$\theta_{rv}\,(\mathrm{m}^3\cdot\mathrm{m}^{-3})$	0.07
$\theta_s\,(\mathrm{m}^3\cdot\mathrm{m}^{-3})$	0.3

$X\,(\%)$ is the mass fraction of salt in an aqueous solution such that

$$X = \frac{m_s}{m_w}100 = \frac{c}{\rho_l}100 \tag{13}$$

where m_s(g) and m_w (g) are the mass of salt and water, $c\,(\mathrm{g}\cdot\mathrm{L}^{-1})$ is the salt concentration, and the density of liquid water here is expressed in units of $\mathrm{g}\cdot\mathrm{L}^{-1}$ (i.e., $\rho_l = 1{,}000\ \mathrm{g}\cdot\mathrm{L}^{-1}$). c is thus given by $10X$. The relationship between freezing point depression and salt concentration from Table 2 is well represented by a second order polynomial function passing through the origin,

$$T_m = p_1 c^2 + p_2 c \tag{14}$$

where $T_m\,(\mathrm{K})$ is the minimum temperature below T_0 where only liquid water is present. p_1 and p_2 are found by fitting Equation 14 to the observed data (Table 2) using linear regression. Following the fitting, the values of p_1 and p_2 were found to be −0.00012544 and −0.05561807, respectively. Solving Equation 14 for c leads to

$$c = \frac{-p_2 - \sqrt{{p_2}^2 + 4p_1T_m}}{2p_1} \tag{15}$$

Now, assuming that this relationship can apply to pore water within a soil control volume, $V(\mathrm{L})$ with a fixed mass of salt, m_s, then we have

$$c = \frac{m_s}{(\theta_l - \theta_r)V} = \frac{c_b}{(\theta_l - \theta_r)} \tag{16}$$

where $c_b\,(\mathrm{g}\cdot\mathrm{L}^{-1})$ is the bulk solute concentration in the soil, that is, mass of salt per soil control volume, $m_s\ /\ V$. Note that in Equation 16 we subtract the residual water content from θ_l which is equivalent to assuming that solutes are not freely exchanged between the free pore water and the residual water in the soil. We tested our models with and without this assumption and found that the predicted behavior of the model was more consistent with observed SFCs (which do not, normally, freeze to zero liquid water content) with this assumption. In our salt exclusion model, we assume that all of the pore water remains liquid until the temperature drops to T_m, corresponding to the solute concentration, c using Equation 14. As the temperature drops below T_m, the concentration of salt in liquid water increases according to Equation 15, and we find the liquid water content to sustain this concentration from Equation 16. Thus combining Equations 15 and 16 and substituting the maximum possible liquid water content in the soil, θ_m, for θ_l we have

$$\theta_m = \theta_r + \frac{2c_bp_1}{-p_2 - \sqrt{{p_2}^2 + 4p_1T_d}} \tag{17}$$

Equation 17 returns the maximum possible liquid water content for a given bulk solute concentration and soil temperature. The actual liquid water content, then, is given by

$$\theta_l = \begin{cases} \theta_t & \theta_m \geq \theta_t \\ \theta_m & \theta_m < \theta_t \end{cases} \tag{18}$$

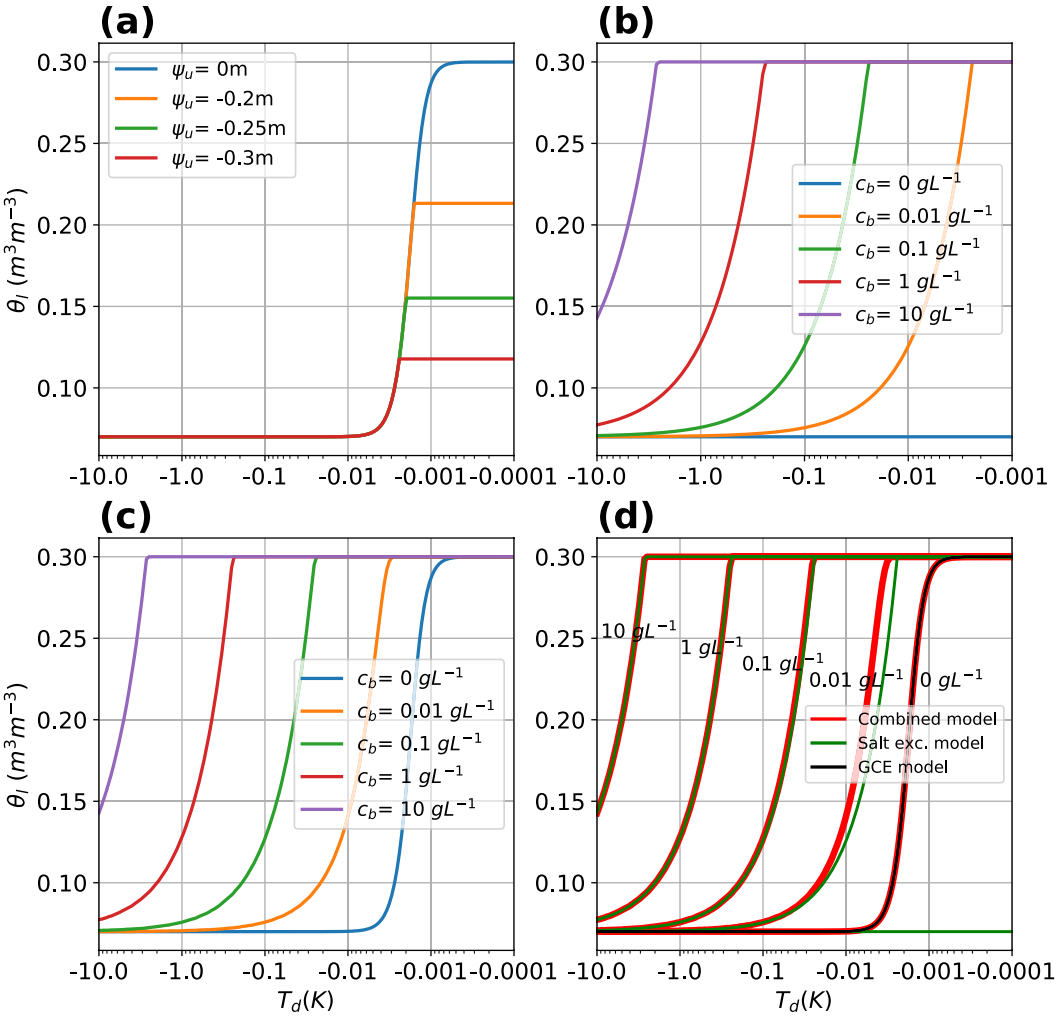

Figure 2. (a) Generalized Clapeyron Equation model simulations with arbitrary soil parameters and differing ψ_u (or differing total water contents), (b) simulated results for the salt exclusion model using arbitrary parameters and differing salt mass (per bulk soil volume), (c) simulations for the combined capillary salt model using arbitrary soil parameter and differing salt mass (per bulk soil volume), and (d) comparing the outcomes of the 3 models.

where again θ_l is the total water content corresponding to ψ_u. Equations 17 and 18 thus define an SFC relationship that predicts θ_l based on the total water content (which can be given by Equation 11), soil temperature and the bulk soil solute concentration.

2.3.3. Combined Model

Models in the literature that combine the effects of solutes and capillary/adsorption effects on freezing point depression do so by summing the osmotic and matric potentials (Schafer & Beier, 2017; Spaans & Baker, 1996; Zhou et al., 2018). We instead assume here that the solute depression effect acts to lower the temperature at which freezing is initiated in the absence of capillary effects. Equation 7 (the GCE equation) is therefore integrated between the new limits $\left(T = T_m, \psi = 0\right)$ and $\left(T = T_f, \psi = \psi_f\right)$, thus giving

$$\psi_f = \frac{L}{g}\ln\left(\frac{T_f}{T_m}\right) = \frac{L}{g}\ln\left(\frac{T_0 + T_d}{T_m}\right) \tag{19}$$

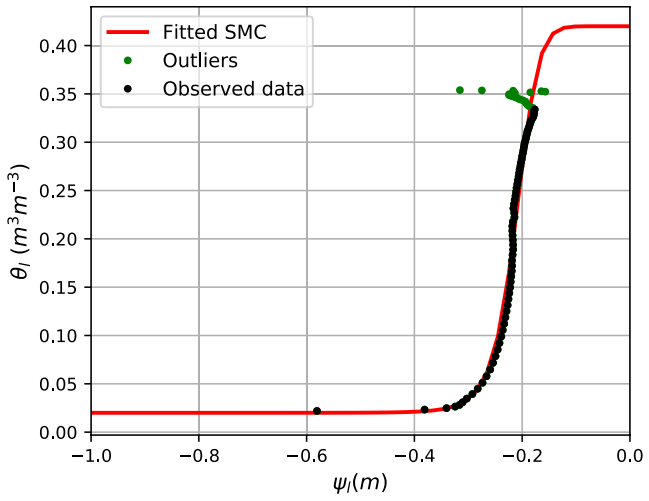

Figure 3. The soil moisture characteristic curve of silica sand measured using the HYPROP apparatus (black dots) and fitted to the van Genuchten model (solid red line).

The challenge we now face is that we have a circular problem: θ_l depends on ψ_f (Equation 10) which depends on T_m (Equation 19) which depends on c(Equation 14) which depends on θ_l (Equation 16). We therefore solve this problem using an iterative approach, as follows: for a given ψ_u, T and c_b we first guess the liquid water content θ_{l0}; next we use Equations 10, 19, 14, and 16 in sequence to calculate a new liquid water content, θ_{l1}; next we check the squared error $\left(\theta_{l0} - \theta_{l1}\right)^2$ against some tolerance value (10^{-8}) and if the error is too large we reset our initial guess to $\theta_{l0} = \omega\theta_{l1} + \left(1 - \omega\right)\theta_{L0}$ and repeat these steps until convergence. Here ω is a relaxation factor (0–1) that is, adjusted to improve the speed of convergence. Using this approach we were able to obtain stable convergence with $\omega = 0.05$. It is possible that an improved mathematical solution procedure could be obtained for this problem, but for our purposes, this approach is adequate.

2.3.4. Behavior of the Alternative Models

The three models described above were run using arbitrary soil parameters (Table 3) to produce SFCs plotted in Figure 2. The capillary effect model (Figure 2a) describes the SFC for soils with no solute effects, and was run with different total water contents (represented using different equivalent unfrozen matric potentials ψ_u of 0, –0.2, –0.25, and –0.3 m). The soil water remains liquid with reducing soil temperature until it reaches a certain depressed temperature when freezing commences, shown by the decrease in liquid water content with temperature. The salt exclusion model and combined model were both run for saturated conditions with changing bulk solute concentrations ($c_b = 0$ g·L^{-1}, 0.01 g·L^{-1}, 0.1 g·L^{-1}, 1 g·L^{-1}, and 10 g·L^{-1}). The simulation results shows that the salt exclusion model (Figure 2b) predicts enhanced freezing point depression with increasing salt concentrations, or in other words, more liquid water remains at the same temperature for higher salt concentrations (represented by a shift of the curve to the left-hand side of the plot). This model simulates no freezing point depression if the solute concentration is zero—a condition that does not occur in real soils. The combined model (Figure 2c) behaves the same as the salt exclusion model at high solute concentrations, and the same as the GCE model with zero solute concentration, as would be expected. For the arbitrary soil that these simulations were run for, the salt exclusion model and combined model only differed noticeably when the solute concentration was less than 0.1 g·L^{-1} (Figure 2d).

3. Results and Discussion

3.1. Laboratory Experiments

The observed SMC for the silica sand that was measured in a laboratory drying experiment, as described in Section 2.1, is shown in Figure 3. The VGN model was fit to these data. The observed data did not extend up to saturation (i.e., $\psi_u = 0$) which is probably because the soil was not completely saturated at the start of the experiment. The saturated moisture content (θ_s) was set to be equal to the measured porosity of the soil (0.42 m^3·m^{-3}) The residual moisture content (θ_r) was identified visually from Figure 3. The parameters

Table 4
Fitted Parameters and Root Mean Square Error for the Soil Moisture Characteristic Curve of the Silica Sand

VGN parameters	Value
α (m^{-1})	−4.79
n	10.11
m	0.90
θ_{rv} (m^3·m^{-3})	0.02
θ_s (m^3·m^{-3})	0.42

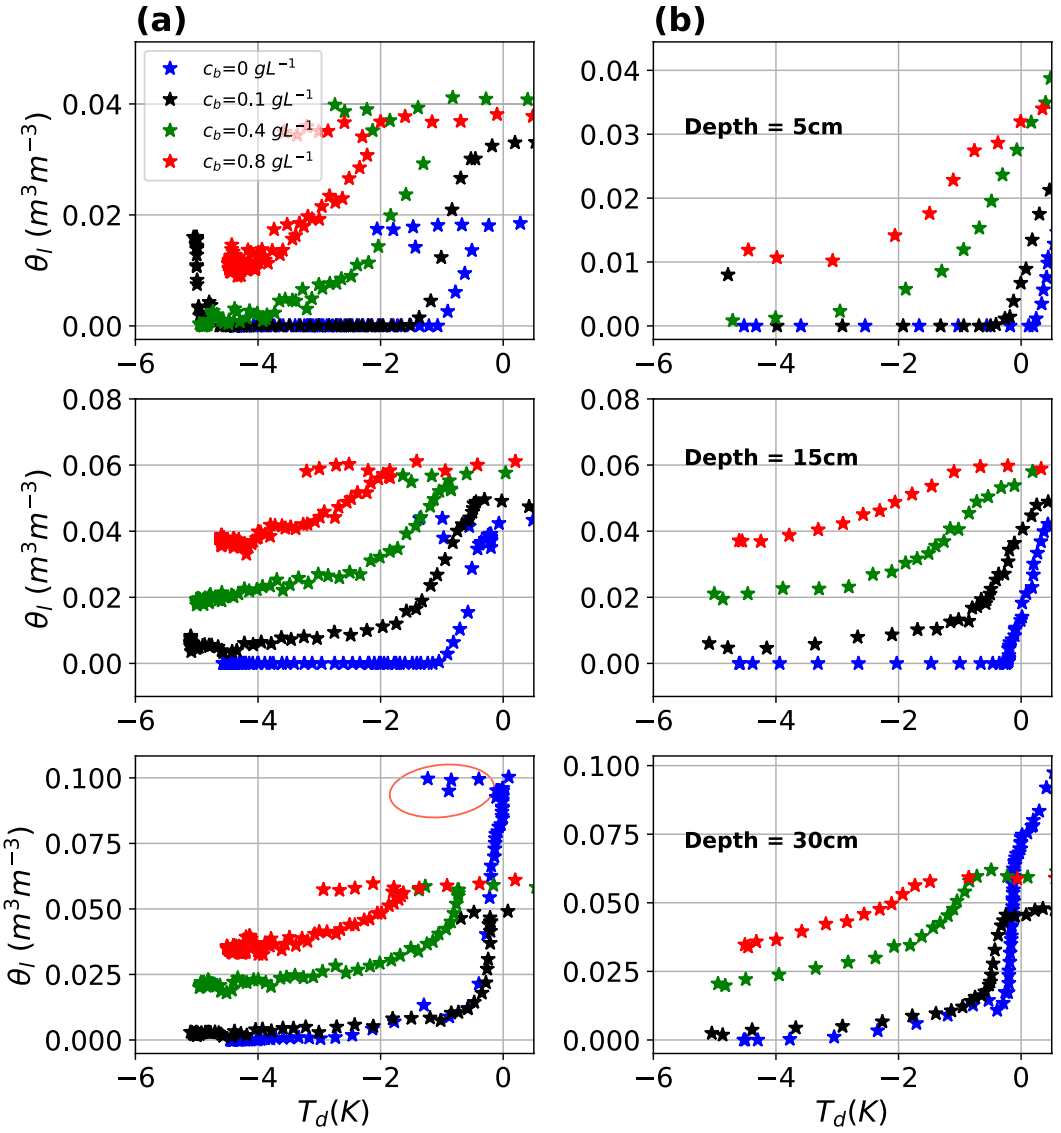

Figure 4. Soil freezing characteristic curves of the silica sand at different salt concentrations at a target moisture content of 0.05 $m^3 \cdot m^{-3}$ (a) freezing curves for different soil depth, and (b) thawing curves for different soil depth.

n, m, and α (Table 4) were obtained by optimization, minimizing the root mean squared error (RMSE) in water content. After fitting the RMSE was 0.017. The green dots are observed data points from the start of the experiment and were excluded from the fitting because they were not consistent with a typical SMC curve. This was likely due to non-equilibrium conditions in the soil sample at the beginning of the experiment. Judging from the results (Figure 3), this soil has poor water retention, and drains rapidly as the matric potential drops below about −0.1 m. The soil reaches its residual moisture content (about 0.02 $m^3 \cdot m^{-3}$) at a matric potential of about −0.38 m. This result is typical of coarse textured soils that lose moisture rapidly due to their large pore sizes.

SFCs measured in the laboratory for the same sand and with varying pore-water dissolved salt (NaCl) concentrations are plotted in Figure 4 (at a target moisture content of 0.05 $m^3 \cdot m^{-3}$) and Figure 5 (at a target moisture content of 0.24 $m^3 \cdot m^{-3}$). The results show, as expected, that higher salinity results in enhanced freezing point depression (curves shift to the left), or in other words, for the same temperature more liquid water is retained in the soil at higher salt concentrations. The results also reveal the phenomenon of supercooling during freezing (depicted by the red-colored ring in the third plot on the third row of Figure 4a).

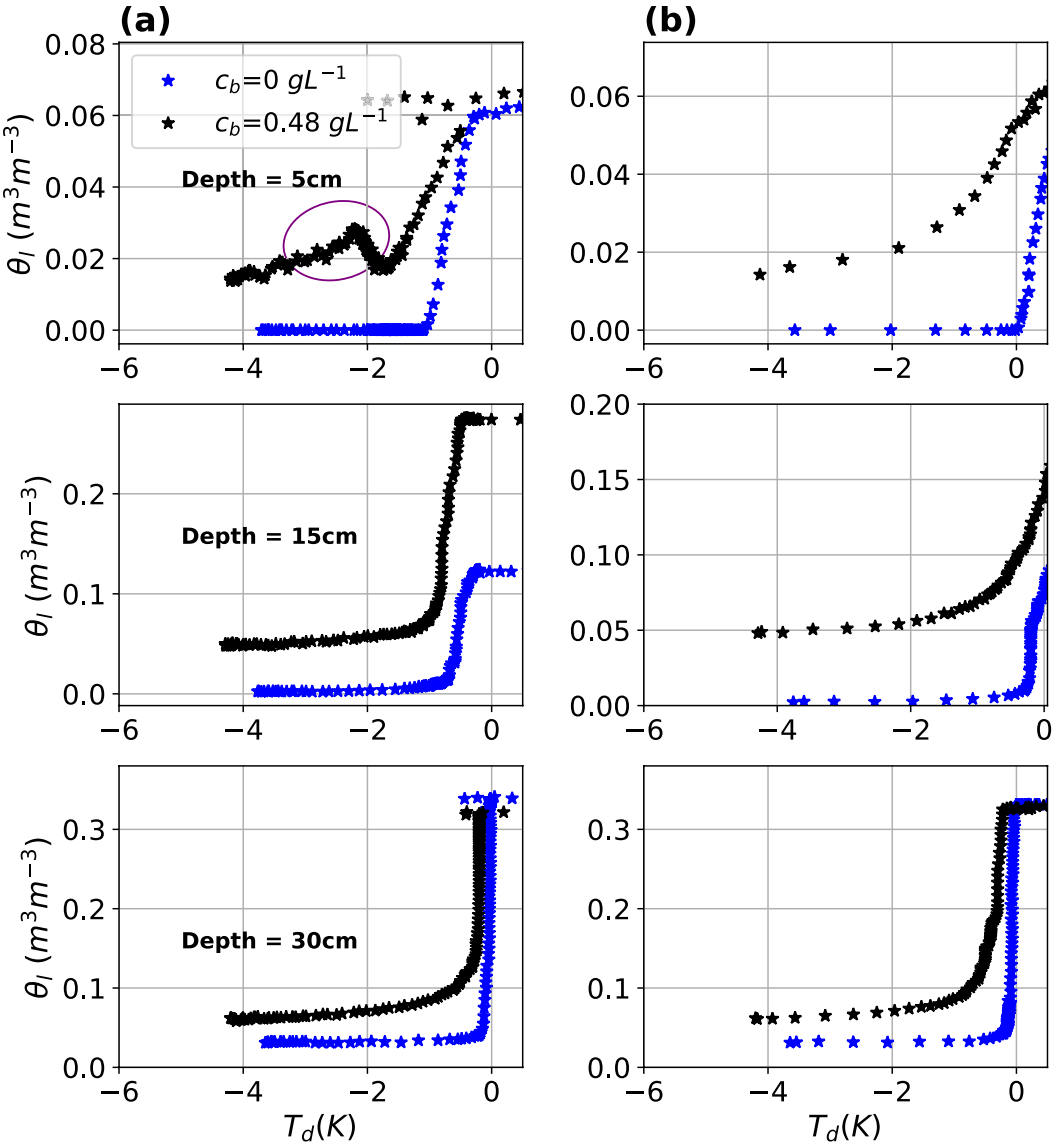

Figure 5. Soil freezing characteristic curves of the silica sand at different salt concentrations at a target moisture content of 0.24 $m^3 \cdot m^{-3}$ (a) freezing curves for different soil depth, and (b) thawing curves for different soil depth.

The temperature of the soil decreased to what is termed as the temperature of spontaneous nucleation (T_{SN}) (Kozlowski, 2009; Zhou et al., 2020) without a change in moisture content. Supercooling is a metastable stage in freezing and is common in laboratory experiments. T_{SN} is the temperature at which a stable ice nucleus for ice crystallization forms in a freezing soil (Kozlowski, 2009). After reaching the T_{SN} there is a release of latent heat that warms the soil to its freezing point where freezing begins (Kozlowski, 2009; Ren & Vanapalli, 2020; Zhou et al., 2020). The supercooling effect is absent in the thawing curves (Figures 4b and 5b), which is as expected. In Figure 5a there are some spurious data, indicated by the purple ring, which we assume is due to some disturbance to the probe, and hence this is ignored.

3.2. Field Experiment

Figure 6 is the results for the SDN site: SMCs fitted to the VGN model (solid pink line) (Figure 6a), freezing curves (Figure 6b) and thawing curves (Figure 6c). The results show that the SMCs for the different years are different. Some specific reasons for this observation may include (a) shrinking or swelling of the soils,

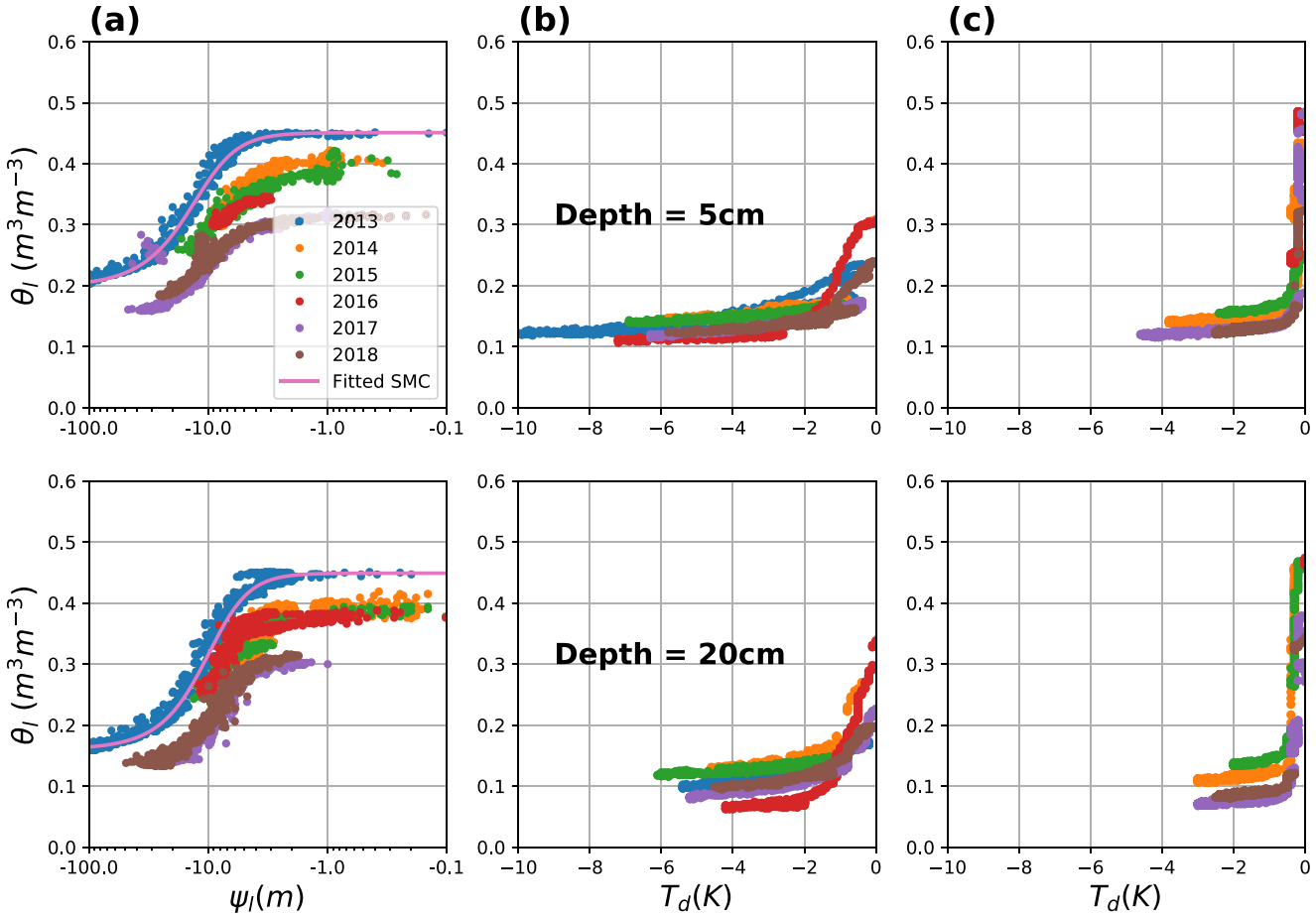

Figure 6. Results for the St Denis National Wildlife Area field site; (a) soil moisture characteristic curves for different years fitted to the van Genuchten model (solid purple line), (b) freezing curves for different years, and (c) thawing curves for different years.

particularly because the soil here is rich in clay, and (b) the shifting of measuring instruments. The 2013 curves are used in all analysis, since the 2013 curves are wetter than the other years and looks reasonably consistent at all the soil depths. The curves were fitted to the VGN model by minimizing the RMSE, which is calculated from the difference between the observed moisture content and the predicted moisture content from the VGN model (fitting parameters values are documented in Table 5). The results also shows that the total water content at the onset of freezing (Figure 6b) was significantly lower than the total water content at the end of the thawing (Figure 6c). The pre-freeze up water content depends on how much rainfall fell in the late summer or fall months. The post thaw water content depends on moisture migration to the frozen soil over the winter months (cryosuction, which we cannot directly observe, since this water would refreeze and as ice it would be invisible to the dielectric probes), and infiltration of snowmelt that occurs before the soil thaws. The SMC of the OJP site and the VGN model (red line) is shown in Figure 7a (find parameter values in Table 6). Similar to the laboratory soil, the OJP soil is coarse-textured and loses moisture rapidly.

Table 5
Fitted Parameter Values of VGN for St Denis National Wildlife Area Site

Soil depth	Year	$\alpha(m^{-1})$	n	m	$\theta_r(m^3{\cdot}m^{-3})$	$\theta_s(m^3{\cdot}m^{-3})$	RMSE
5 cm	2013	0.094	2.55	0.61	0.198	0.45	0.0095
20 cm	2013	0.12	2.72	0.63	0.16	0.45	0.0119
50 cm	2013	0.094	2.55	0.61	0.198	0.45	0.0095

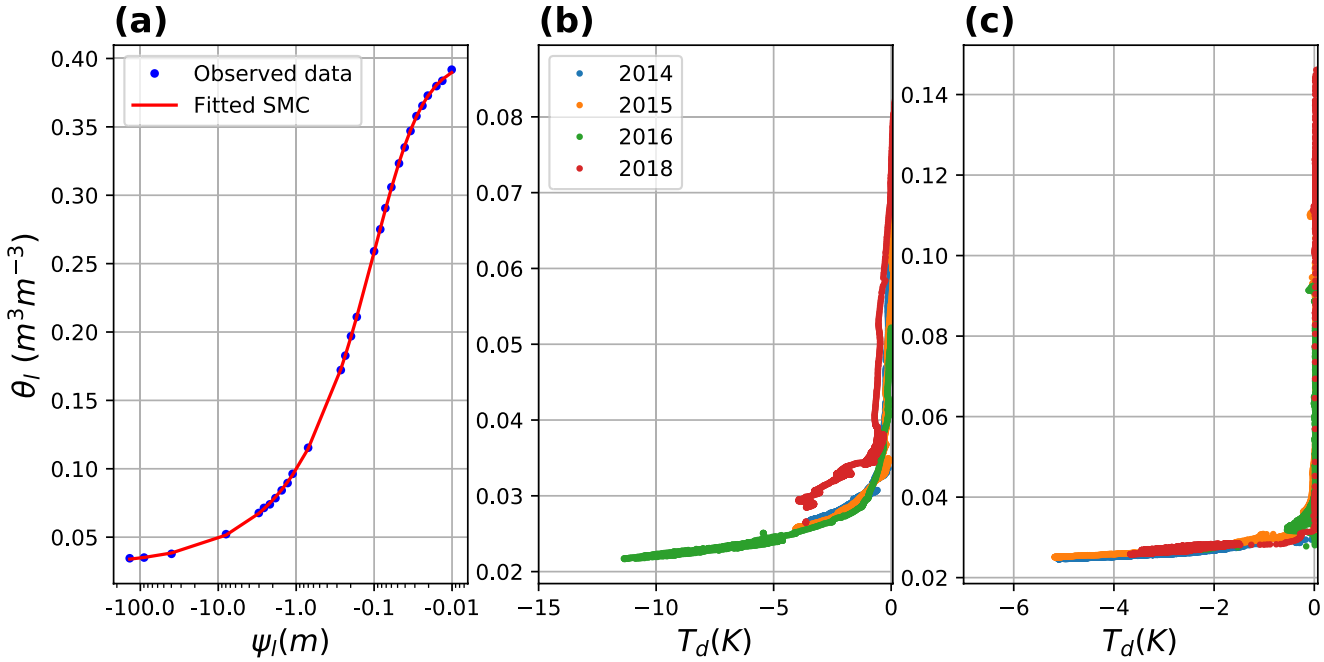

Figure 7. Results for the Old Jack Pine field site; (a) soil moisture characteristic curve fitted to the van Genuchten model (solid red line), (b) freezing curves for different years for the top 15 cm depth, and (c) thawing curves for different years for the top 15 cm depth.

Again, we see here that the thawing curve (Figure 7c) ends up wetter than the freezing curves (Figure 7b), which we attribute solely to snowmelt infiltration. The OJP site has very low moisture content; hence moisture migration may not be practical.

3.3. Model Performance

Models were run for each of the laboratory and field experiments, to reproduce the SFCs. We found that in many cases, the residual water content, θ_r, was lower for the freezing curves (SFCs) compared with the drying curves (SMCs). This could be an artifact of the probe, but we suspect that this could be a real phenomenon. This suggests that the minimum pore size for drying is larger than the minimum pore size for freezing. Because of this, we adjusted θ_r for our models to match the SFC data. Similarly, in their model Evans et al. (2020) allow for the soil residual water content to differ during freezing versus drying.

The validation results for the three models (capillary, salt exclusion, and the combined model) using laboratory measured SFCs are presented in Figures 8 and 9. Here the models were compared with observations from 30 cm depth because the shallower probes (5 and 15 cm depths) froze rapidly and were possibly not in thermodynamic equilibrium, and hence may overpredict the freezing point depression in the soil. The bulk soil salt concentrations were assumed to remain constant for the duration of the experiment, that is, we ignore any potential salt redistribution in the soil profile.

Figure 8 presents the results for the case where no salt was added to the soil in the experiment. In Figure 8a, a value of $c_b = 0$ is used in the salt exclusion and combined models, and the performance of the three models are compared. As expected, the capillary and combined models are identical and the salt exclusion model predicts no freezing point depression. The performance of the GCE model is poor, which suggests

Table 6
Fitted Parameter Values of VGN for Old Jack Pine Site

Parameter	$\alpha(m^{-1})$	n	m	$\theta_r(m^3 \cdot m^{-3})$	$\theta_s(m^3 \cdot m^{-3})$	RMSE
Value	19.44	1.6	0.4	0.03	0.4	0.00076

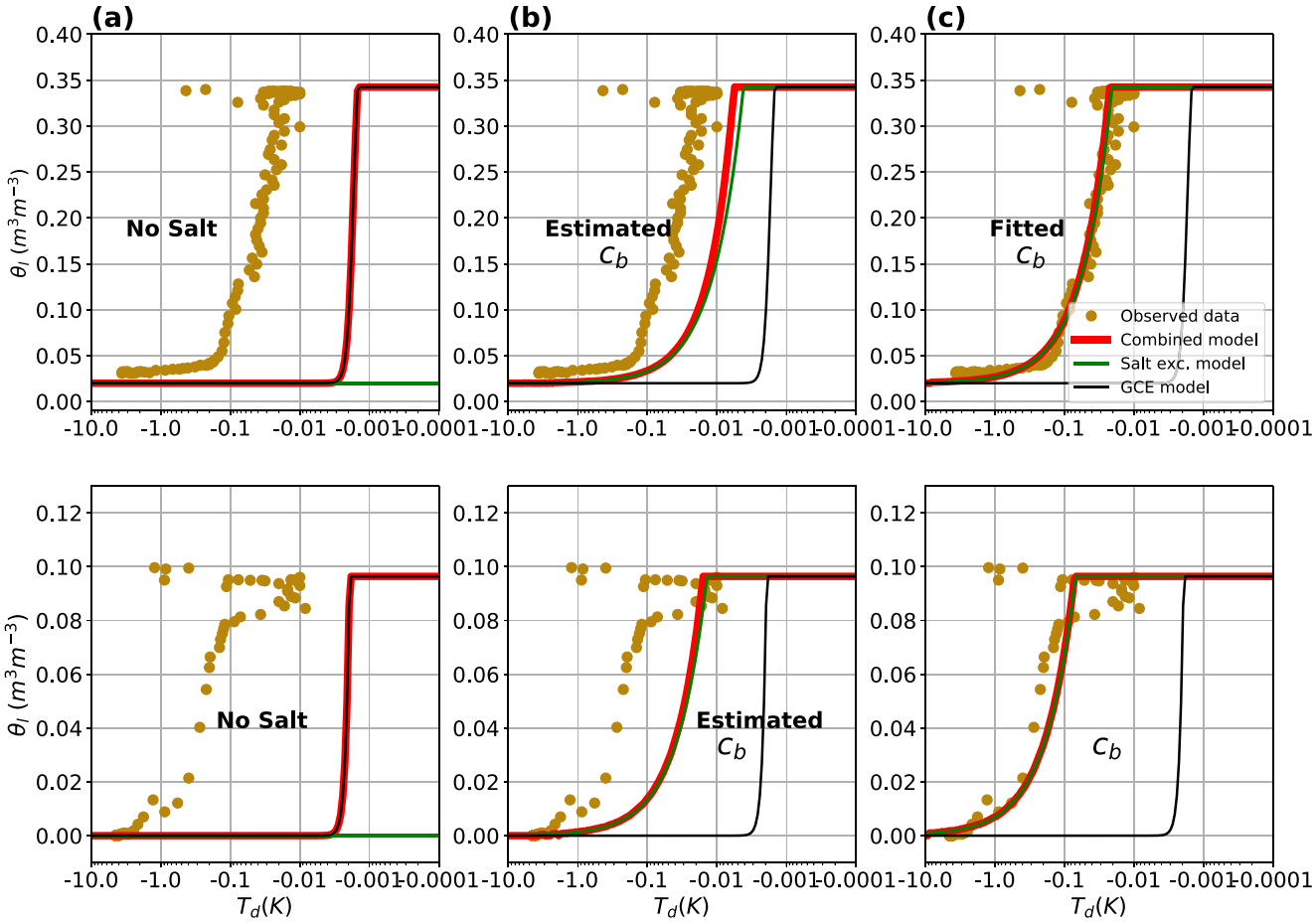

Figure 8. Performance of the three models (capillary, salt-exclusion, and combined model) against laboratory observed soil freezing characteristic curves at 30 cm depth with no salt added: (a) salt exclusion and combined models with no fitting, $c_b = 0\,\mathrm{g{\cdot}L^{-1}}$; (b) salt exclusion and combined models with estimated $c_b = 0.024\,\mathrm{g{\cdot}L^{-1}}$ and (c) salt exclusion and combined models fitted to the data with $c_b = 0.12\,\mathrm{g{\cdot}L^{-1}}$. Upper panel is results for higher antecedent moisture content and lower panel is results for lower antecedent moisture content.

that the assumptions within the GCE are inappropriate for this soil. Despite our efforts to minimize solutes (using de-ionized water and pure silica sand), the soil pore water may still contain some amounts of dissolved salts, that may result in higher depression of the freezing point in the SFCs. This was tested by mixing 100 g of sand with 100 ml of deionized water and measuring the electric conductivity (EC) after the mixture was stirred for about 5 min and allowed to settle. A calibrated conductivity meter gave a reading of 19 μ S·cm^{-1}, equivalent to $c_b = 0.024\,\mathrm{g{\cdot}L^{-1}}$ (the EC was converted to c_s, i.e., TDS, by multiplying by 0.64, Chang et al., 1983). Note that this is just an estimate of the salt concentration in the sand since the actual conversion of EC to TDS depends on the activity of the different ions in the sand. When this concentration was used in the combined and salt exclusion models their performance was markedly improved, Figure 8b, though the model still did not fit the observations. These models could be made to fit the observations well by using a value of $c_b = 0.12\,\mathrm{g{\cdot}L^{-1}}$, Figure 8c, determined by manual calibration. This is likely an unrealistically high solute concentration for this experiment. It must be noted that the temperature in Figure 8 is on a log-scale, and the errors in Figures 8a and 8b are smaller than the reported error tolerance of the temperature observations with the probe (±0.3 K).

The results for the experiments where a fixed mass of NaCl salt was added to the soil are shown in Figure 9. The poor performance of the GCE model was unchanged, but both the salt exclusion and the combined model performed well without calibration or refinement. Since the predictions from the combined and

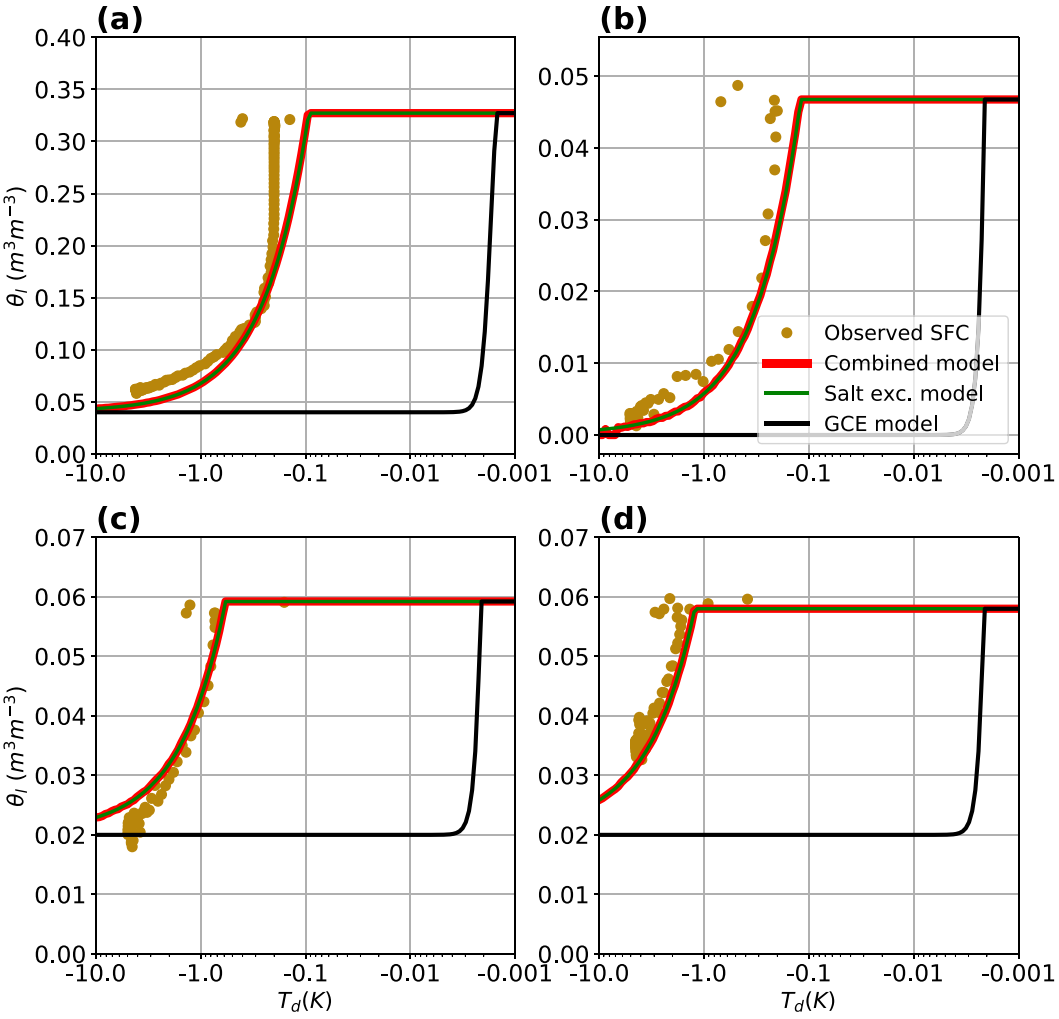

Figure 9. Performance of the three models (capillary, salt-exclusion, and combined models) against laboratory observed soil freezing characteristic curves at 30 cm depth for different salt concentrations and water contents: (a) c_b = 0.48 g·L^{-1}; high moisture content (b) c_b =0.1 g·L^{-1}; low moisture content (c) c_b =0.4 g·L^{-1}; low moisture content, and (d) c_b = 0.8 g·L^{-1}; low moisture content.

salt exclusion models were identical, this implies that the SFCs here are completely dominated by the salt exclusion effect.

Figures 10 and 11 show the performance of the three models at the SDN and OJP field sites, respectively. The models were first run without salt ($c_b = 0$, Figures 10a and 11a) and then by adding arbitrary amounts of salt to fit the models to the observed SFCs (Figures 10b and 11b). Note that at SDN the largest adjustments to θ_r were made, and it is clear from the observations alone (Figure 6) that there are significant differences in the lower limit of the liquid water content for drying and freezing. The model results show that for both field sites (SDN and OJP), the GCE model and the identical combined model with zero salt underestimated freezing point depression (Figures 10a and 11a). This is less surprising than for the laboratory experiments because we expect significant amounts of dissolved salts in these field soils. The underestimation is smaller at the OJP site (Figure 11a) than at the SDN site (Figure 10a), which was also expected because the OJP site has less saline soil, and thus, the salt exclusion effect should be smaller. Again, the salt exclusion model failed as expected when no salt was added to the model. In Figures 10b and 11b salt was added to the model to fit the observed SFCs, and here both the salt exclusion and the combined model did well in predicting the observed SFCs for both field sites. Comparing the average salt concentration used in the fitting run for

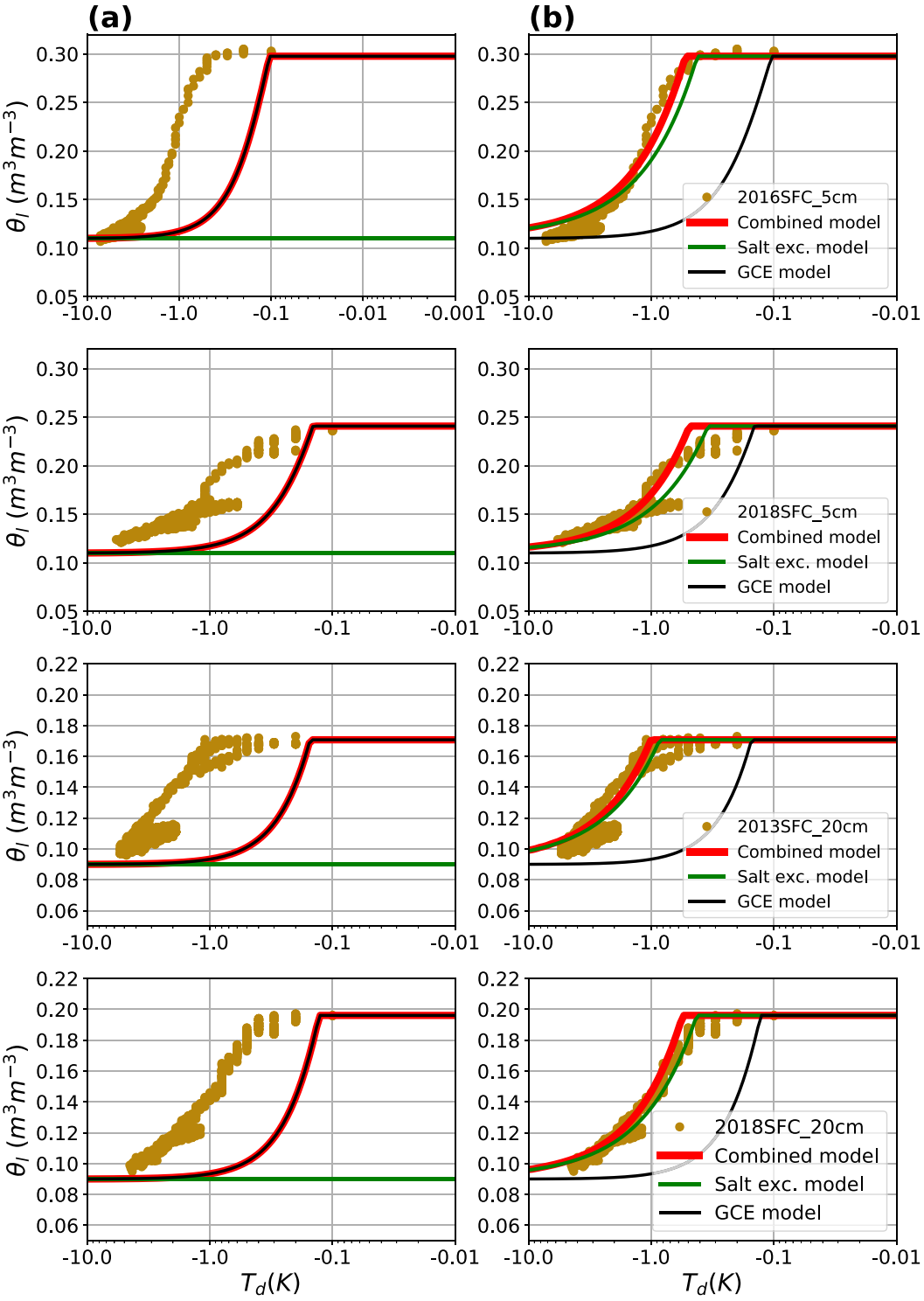

Figure 10. Performance of the three models (capillary, salt-exclusion, and combined capillary salt model) against observed soil freezing characteristic curve's (SFCs) for St Denis National Wildlife Area site; (a) models applied without salt and, (b) model fitted to the observed SFCs by adjusting the salt masses.

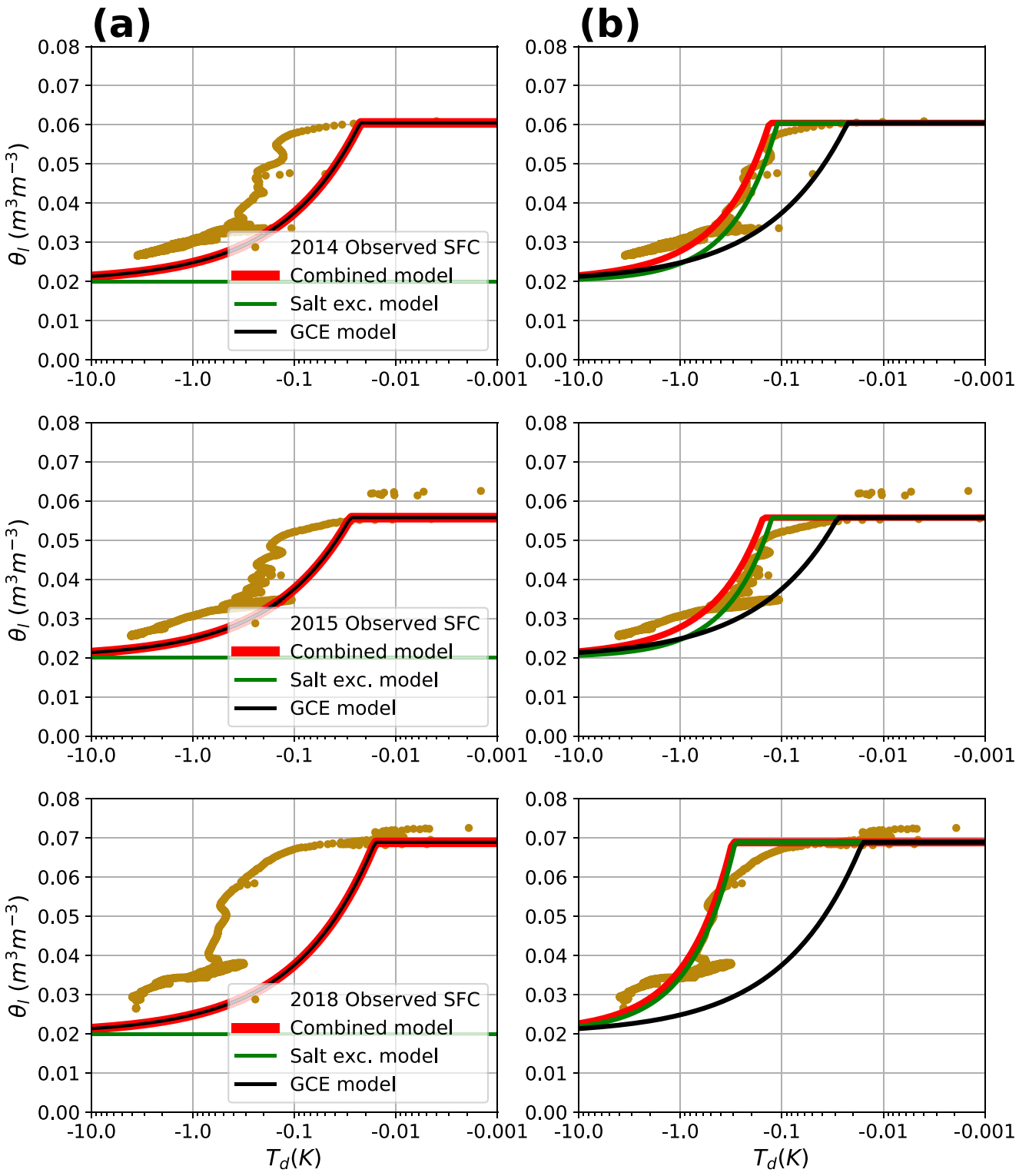

Figure 11. Performance of the three models (capillary, salt-exclusion, and combined capillary salt model) against observed soil freezing characteristic curve's (SFCs) for Old Jack Pine site; (a) models applied without salt and, (b) model fitted to the observed SFCs by adjusting the salt masses.

Table 7
Bulk Salt Concentration (c_b) Used in the Fitting Runs for the St Denis National Wildlife Area (SDN) and Old Jack Pine (OJP) Field Sites

SDN site		OJP site	
Year and depth	c_b (g·L^{-1})	Year	c_b (g·L^{-1})
2016 5 cm	1.4	2014	0.08
2018 5 cm	0.8	2015	0.08
2013 20 cm	1.2	2018	0.25
2018 20 cm	0.8	–	–
Average	1.05	Average	0.14

the SDN site to those used at the OJP site (Table 7), we see that the SDN site has more salt than the OJP site, which is correct. We cannot directly validate the fitted salt concentrations reported for our field sites in Table 7, but the values for SDN are within the range of electrical conductivities reported by Nachshon et al. (2014) for the soils in the general vicinity of our instrumentation.

4. Conclusions

In this study, SMCs and SFCs were measured for soils with varying texture and salinity in laboratory and field conditions, using dielectric impedance probes to measure the liquid water content. In our seasonally frozen field sites, SFCs have a number of important characteristics, which we summarize conceptually in Figure 12, and describe here: (a) the antecedent water content prior to freezing are normally not saturated, and may in fact be quite dry, meaning that assuming saturated soils for frozen conditions is likely to introduce significant errors; (b) the freezing and thawing curves are distinctly hysteretic (consistent with previously reported curves from Koopmans & Miller, 1966, Tice et al., 1989, and Watanabe & Osada, 2017); and (c) the soils are wetter, and perhaps saturated, at the end of thawing, which is due to a combination of possible soil moisture redistribution by cryosuction during the winter, and snowmelt infiltration during the melt period.

Three alternative models were developed to simulate the SFC: a GCE model; a salt exclusion model; and a combined model. The combined model is shown to be identical to the GCE model when there is no salt in the soil, and identical to the salt exclusion model when salt concentrations are high. The salt exclusion model fails to predict any freezing point depression when there is no salt in the pore water (though such completely salt-free conditions do not exist in real soils). In the salt exclusion and combined model, the effect of adding more salt is to increase the amount of freezing point depression progressively.

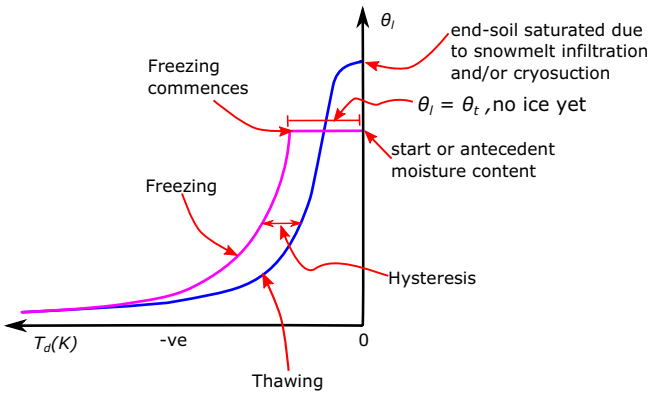

Figure 12. Conceptual diagram depicting the difference between freezing and thawing in frozen soils.

The three alternative models were tested against our observed SFCs. In all cases, we found that the GCE model significantly under-predicted freezing point depression (i.e., the temperature for a given liquid water content is under-predicted, or equivalently, the liquid water content for a given temperature is under-predicted). In the controlled salinity lab experiments, we found excellent agreement between the salt exclusion and combined models, with no fitting (i.e., calibration). However, for the zero salinity case, the models all failed, unless we introduced a small amount of salt. By fitting the model in this way the salt exclusion and combined models performed well. We also found that to define the SFC it was necessary to reduce the residual water content from that used in the SMC, and we speculate that this is a real phenomenon, where ice is able to propagate into smaller pores during freezing than air is during drying.

Our results suggest that, at least for the soils we considered, salt exclusion effects on freezing point depression are more important than capillary effects. The widely used GCE is likely to under-predict freezing point depression. The consequence of this is that for a given subzero temperature, the

equivalent matric potential caused by freezing, as predicted by the GCE, is too low, which in coupled models is likely to lead to significant over estimates of hydraulic gradients associated with cryosuction, and associated numerical instabilities. It would be valuable in future work to explore the consequences of the salt-exclusion model in coupled models. In such models, where the salinity is unknown, but measurements of the SFC are available, the soil bulk concentration, c_b, can be treated as a single fitting parameter to define the SFC.

Data Availability Statement

Data used in this study are available online at https://doi.org/10.20383/102.0391 in the Canadian Federated Research Data Repository (FRDR).

Acknowledgments
This project was funded by the Global Water Futures Program at the Global Institute for Water Security (GIWS) and University of Saskatchewan. We are exceedingly grateful to Dr Christopher Spence from Environment and Climate Change Canada for permitting us to use his laboratory and for his feedback on this work. We thank Cody Millar from the Mine Overlay Site Testing (MOST) facility, University of Saskatchewan, for their help running some analysis on the soil. We are also grateful to Uri Nachshon and Xicai Pan for their work on the installation of the SDN field instrumentation back in 2013 and to Bruce Johnson and all the technicians at the GIWS responsible for collecting and organizing the data sets for the SDN and OJP field sites. We are very grateful to Aaron Mohammed and two anonymous reviewers for their useful feedback and comments on this manuscript.

References

Azmatch, T. F., Sego, D. C., Arenson, L. U., & Biggar, K. W. (2012). Using soil freezing characteristic curve to estimate the hydraulic conductivity function of partially frozen soils. *Cold Regions Science and Technology*, *83–84*, 103–109. https://doi.org/10.1016/j.coldregions.2012.07.002

Bam, E. K. P., Brannen, R., Budhathoki, S., Ireson, A. M., Spence, C., & van der Kamp, G. (2019). Meteorological, soil moisture, surface water, and groundwater data from the St. Denis National Wildlife Area, Saskatchewan, Canada. *Earth System Science Data*, *11*(2), 553–563. https://doi.org/10.5194/essd-2018-125

Bam, E. K. P., & Ireson, A. M. (2019). Quantifying the wetland water balance: A new isotope-based approach that includes precipitation and infiltration. *Journal of Hydrology*, *570*, 185–200. https://doi.org/10.1016/j.jhydrol.2018.12.032

Banin, A., & Anderson, D. M. (1974). Effects of salt concentration changes during freezing on the unfrozen water content of porous materials. *Water Resources Research*, *10*(1), 124–128. https://doi.org/10.1029/WR010i001p00124

Barr, A. G., van der Kamp, G., Black, T. A., McCaughey, J. H., & Nesic, Z. (2012). Energy balance closure at the BERMS flux towers in relation to the water balance of the White Gull Creek watershed 1999–2009. *Agricultural and Forest Meteorology*, *153*, 3–13. https://doi.org/10.1016/j.agrformet.2011.05.017

Breitmeyer, R. J., & Fissel, L. (2017). Uncertainty of soil water characteristic curve measurements using an automated evaporation technique. *Vadose Zone Journal*, *16*(13), 1–11. https://doi.org/10.2136/vzj2017.07.0136

Budhathoki, S. (2018). *Modelling snowmelt infiltration processes in seasonally frozen ground*. Thesis. University of Saskatchewan. Retrieved from https://harvest.usask.ca/handle/10388/8468

Caicedo, B. (2017). Physical modelling of freezing and thawing of unsaturated soils. *Géotechnique*, *67*(2), 106–126. https://doi.org/10.1680/jgeot.15.P.098

Chang, C., Sommerfeldt, T. G., Carefoot, J. M., & Schaalje, G. B. (1983). Relationships of electrical conductivity with total dissolved salts and cation concentration of sulfate-dominant soil extracts. *Canadian Journal of Soil Science*, *63*(1), 79–86. https://doi.org/10.4141/cjss83-008

Christensen, A. F., He, H., Dyck, M. F., Lenore Turner, E., Chanasyk, D. S., Naeth, M. A., & Nichol, C. (2013). In situ measurement of snowmelt infiltration under various topsoil cap thicknesses on a reclaimed site. *Canadian Journal of Soil Science*, *93*(4), 497–510. https://doi.org/10.4141/cjss2012-048

Clark, M. P., Nijssen, B., Lundquist, J. D., Kavetski, D., Rupp, D. E., Woods, R. A., et al. (2015). A unified approach for process-based hydrologic modeling: 2. Model implementation and case studies. *Water Resources Research*, *51*(4), 2515–2542. https://doi.org/10.1002/2015WR017200

Cuenca, R. H., Stangel, D. E., & Kelly, S. F. (1997). Soil water balance in a boreal forest. *Journal of Geophysical Research*, *102*(D24), 29355–29365. https://doi.org/10.1029/97JD02312

Dall'Amico, M., Endrizzi, S., Gruber, S., & Rigon, R. (2011). A robust and energy-conserving model of freezing variably saturated soil. *The Cryosphere*, *5*(2), 469–484. https://doi.org/10.5194/tc-5-469-2011

Evans, S. G., Godsey, S. E., Rushlow, C. R., & Voss, C. (2020). Water tracks enhance water flow above permafrost in Upland Arctic Alaska Hillslopes. *Journal of Geophysical Research: Earth Surface*, *125*(2), e2019JF005256. https://doi.org/10.1029/2019JF005256

Flerchinger, G. N., Seyfried, M. S., & Hardegree, S. P. (2006). Using soil freezing characteristics to model multi-season soil water dynamics. *Vadose Zone Journal*, *5*(4), 1143–1153. https://doi.org/10.2136/vzj2006.0025

Gharedaghloo, B., Berg, S. J., & Sudicky, E. A. (2020). Water freezing characteristics in granular soils: Insights from pore-scale simulations. *Advances in Water Resources*, *143*, 103681. https://doi.org/10.1016/j.advwatres.2020.103681

Haghighi, H., Chapoy, A., & Tohidi, B. (2008). Freezing point depression of electrolyte solutions: Experimental measurements and modeling using the cubic-plus-association equation of state. *Industrial & Engineering Chemistry Research*, *47*(11), 3983–3989. https://doi.org/10.1021/ie800017e

Hansson, K., Šimůnek, J., Mizoguchi, M., Lundin, L.-C., & van Genuchten, M. T. (2004). Water flow and heat transport in frozen soil: Numerical solution and freeze–thaw applications. *Vadose Zone Journal*, *3*(2), 693–704. https://doi.org/10.2136/vzj2004.0693

Hayashi, M. (2013). The cold vadose zone: Hydrological and ecological significance of frozen-soil processes. *Vadose Zone Journal*, *12*(4), 1–8. https://doi.org/10.2136/vzj2013.03.0064

Hayashi, M., van der Kamp, G., & Rudolph, D. L. (1998). Water and solute transfer between a prairie wetland and adjacent uplands, 2. Chloride cycle. *Journal of Hydrology*, *207*(1–2), 56–67. https://doi.org/10.1016/S0022-1694(98)00099-7

He, H., Dyck, M., Zhao, Y., Si, B., Jin, H., Zhang, T., et al. (2016). Evaluation of five composite dielectric mixing models for understanding relationships between effective permittivity and unfrozen water content. *Cold Regions Science and Technology*, *130*, 33–42. https://doi.org/10.1016/j.coldregions.2016.07.006

Ireson, A. M., Barr, A. G., Johnstone, J. F., Mamet, S. D., Van Der Kamp, G., Whitfield, C. J., et al. (2015). The changing water cycle: The boreal plains ecozone of Western Canada. *Wiley Interdisciplinary Reviews: Water*, *2*(5), 505–521. https://doi.org/10.1002/wat2.1098

Jin, X., Yang, W., Gao, X., Zhao, J.-Q., Li, Z., & Jiang, J. (2020). Modeling the unfrozen water content of frozen soil based on the absorption effects of clay surfaces. *Water Resources Research*, *56*(12), e2020WR027482. https://doi.org/10.1029/2020WR027482

Kelleners, T. J., & Norton, J. B. (2012). Determining water retention in seasonally frozen soils using hydra impedance sensors. *Soil Science Society of America Journal*, *76*(1), 36–50. https://doi.org/10.2136/sssaj2011.0222
Kelleners, T. J., Paige, G. B., & Gray, S. T. (2009). Measurement of the dielectric properties of wyoming soils using electromagnetic sensors. *Soil Science Society of America Journal*, *73*(5), 1626–1637. https://doi.org/10.2136/sssaj2008.0361
Kelleners, T. J., & Verma, A. K. (2010). Measured and modeled dielectric properties of soils at 50 Megahertz. *Soil Science Society of America Journal*, *74*(3), 744–752. https://doi.org/10.2136/sssaj2009.0359
Koopmans, R. W. R., & Miller, R. D. (1966). Soil freezing and soil water characteristic curves. *Soil Science Society of America Journal*, *30*(6), 680–685. https://doi.org/10.2136/sssaj1966.03615995003000060011x
Kozlowski, T. (2009). Some factors affecting supercooling and the equilibrium freezing point in soil–water systems. *Cold Regions Science and Technology*, *59*(1), 25–33. https://doi.org/10.1016/j.coldregions.2009.05.009
Kurylyk, B. L., & Watanabe, K. (2013). The mathematical representation of freezing and thawing processes in variably saturated, non-deformable soils. *Advances in Water Resources*, *60*, 160–177. https://doi.org/10.1016/j.advwatres.2013.07.016
Mohammed, A. A., Kurylyk, B. L., Cey, E. E., & Hayashi, M. (2018). Snowmelt infiltration and macropore flow in frozen soils: Overview, knowledge gaps, and a conceptual framework. *Vadose Zone Journal*, *17*(1), 180084. https://doi.org/10.2136/vzj2018.04.0084
Nachshon, U., Ireson, A., van der Kamp, G., Davies, S. R., & Wheater, H. S. (2014). Impacts of climate variability on wetland salinization in the North American prairies. *Hydrology and Earth System Sciences*, *18*(4), 1251–1263. https://doi.org/10.5194/hess-18-1251-2014
Nazarbakhsh, M., Ireson, A. M., & Barr, A. G. (2020). Controls on evapotranspiration from jack pine forests in the Boreal Plains ecozone. *Hydrological Processes*, *34*(4), 927–940. https://doi.org/10.1002/hyp.13674
Oquist, M. G., Sparrman, T., Klemedtsson, L., Drotz, S. H., Grip, H., Schleucher, J., & Nilsson, M. (2009). Water availability controls microbial temperature responses in frozen soil CO_2 production. *Global Change Biology*, *15*(11), 2715–2722. https://doi.org/10.1111/j.1365-2486.2009.01898.x
Painter, S. L., & Karra, S. (2014). Constitutive model for unfrozen water content in subfreezing unsaturated soils. *Vadose Zone Journal*, *13*(4), 1–8. https://doi.org/10.2136/vzj2013.04.0071
Patterson, D. E., & Smith, M. W. (1985). Unfrozen water content in saline soils: Results using time-domain reflectometry. *Canadian Geotechnical Journal*, *22*(1), 95–101. https://doi.org/10.1139/t85-009
Pekrioglu Balkis, A. (2019). Determination of SWRC for unsaturated sands, comparative study – Filter paper method versus hanging column technique. *European Journal of Science and Technology* (16), 403–413. https://doi.org/10.31590/ejosat.539620
Pires, L. F., Brinatti, A. M., & Saab, S. C. (2015). Experimental method to determine some physical properties in physics classes. *Revista Brasileira de Ciência do Solo*, *39*(5), 1507–1512. https://doi.org/10.1590/01000683rbcs20140766
Ren, J., & Vanapalli, S. K. (2019). Comparison of soil-freezing and soil-water characteristic curves of two Canadian soils. *Vadose Zone Journal*, *18*(1), 1–14. https://doi.org/10.2136/vzj2018.10.0185
Ren, J., & Vanapalli, S. K. (2020). Effect of freeze–thaw cycling on the soil-freezing characteristic curve of five Canadian soils. *Vadose Zone Journal*, *19*(1), e20039. https://doi.org/10.1002/vzj2.20039
Rohatgi, A. (2015). *WebPlotDigitizer user manual version 3.9* (p. 23).
Schafer, H. L., & Beier, N. A. (2017). *Development of soil freezing characteristic curves for fluid fine tailings using TDR*. Geo Ottawa 2017.
Schofield, R. K. (1935). The pF of the water in soil. *Third International Congress of Soil Science*, *2*, 37–48.
Seyfried, M. S., & Murdock, M. D. (2004). Measurement of soil water content with a 50-MHz soil dielectric sensor. *Soil Science Society of America Journal*, *68*(2), 394–403. https://doi.org/10.2136/sssaj2004.3940
Spaans, E. J. A. (1994). *The soil freezing characteristic: Its measurement and similarity to the soil moisture characteristic*. PhD thesis. University of Michigan.
Spaans, E. J. A., & Baker, J. M. (1996). The soil freezing characteristic: Its measurement and similarity to the soil moisture characteristic. *Soil Science Society of America Journal*, *60*, 13–19. https://doi.org/10.2136/sssaj1996.03615995006000010005x
Stevens Water Monitoring Systems Inc. (2007). *The Hydra Probe® soil sensor, user's manual*, 1–63.
Susha Lekshmi, S. U., Singh, D. N., & Shojaei Baghini, M. (2014). A critical review of soil moisture measurement. *Measurement*, *54*, 92–105. https://doi.org/10.1016/j.measurement.2014.04.007
Teng, J. (2020). Parameterization of soil freezing characteristic curve for unsaturated soils. *Cold Regions Science and Technology*, *8*. https://doi.org/10.1016/j.coldregions.2019.102928
Tice, A. R., Black, P. B., & Berg, R. L. (1989). Unfrozen water contents of undisturbed and remolded Alaskan silt. *Cold Regions Science and Technology*, *17*(2), 103–111. https://doi.org/10.1016/S0165-232X(89)80001-1
van Genuchten, M. (1980). A closed-form equation for predicting the hydraulic conductivity of unsaturated soils 1. *Soil Science Society of America Journal*, *44*(5), 892–898. https://doi.org/10.2136/sssaj1980.03615995004400050002x
Watanabe, K., & Mizoguchi, M. (2002). Amount of unfrozen water in frozen porous media saturated with solution. *Cold Regions Science and Technology*, *34*(2), 103–110. https://doi.org/10.1016/S0165-232X(01)00063-5
Watanabe, K., & Osada, Y. (2017). Simultaneous measurement of unfrozen water content and hydraulic conductivity of partially frozen soil near 0°C. *Cold Regions Science and Technology*, *142*, 79–84. https://doi.org/10.1016/j.coldregions.2017.08.002
Wen, Z., Ma, W., Feng, W., Deng, Y., Wang, D., Fan, Z., & Zhou, C. (2012). Experimental study on unfrozen water content and soil matric potential of Qinghai-Tibetan silty clay. *Environmental Earth Sciences*, *66*(5), 1467–1476. https://doi.org/10.1007/s12665-011-1386-0
Williams, P. J. (1964). Unfrozen water content of frozen soils and soil moisture suction. *Géotechnique*, *14*(3), 231–246. https://doi.org/10.1680/geot.1964.14.3.231
Williams, P. J. (1970). *Properties and behaviour of freezing soils* (pp. 72–79). Norwegian Geotechnical Institute. https://doi.org/10.1016/b978-0-08-016194-5.50009-8
Williams, P. J., & Smith, M. W. (1989). *The frozen earth*. Cambridge University Press.
Yan, G., Li, Z., Bore, T., Scheuermann, A., Galindo-Torres, S., & Li, L. (2017). *The measurement of primary drainage curve using hanging column and large soil column test*. ResearchGate. Retrieved from https://www.researchgate.net/publication/318734619
Zhang, C., & Liu, Z. (2018). Freezing of water confined in porous materials: Role of adsorption and unfreezable threshold. *Acta Geotechnica*, *13*(5), 1203–1213. https://doi.org/10.1007/s11440-018-0637-6
Zhou, J., Meng, X., Wei, C., & Pei, W. (2020). Unified soil freezing characteristic for variably-saturated saline soils. *Water Resources Research*, *56*(7), e2019WR026648. https://doi.org/10.1029/2019WR026648
Zhou, J., Wei, C., Lai, Y., Wei, H., & Tian, H. (2018). Application of the generalized clapeyron equation to freezing point depression and unfrozen water content. *Water Resources Research*, *54*(11), 9412–9431. https://doi.org/10.1029/2018WR023221